Study of a Surface State in a Ag-Au Superlattice Gap

T. Miller and T.-C. Chiang

Department of Physics, University of Illinois at Urbana-Champaign, 1110 West Green Street, Urbana, Illinois 61801 and Materials Research Laboratory, University of Illinois at Urbana-Champaign, 104 South Goodwin Avenue, Urbana, Illinois 61801

(Received 25 October 1991)

Ag-Au(111) superlattices are examined with angle-resolved photoemission. A Shockley-type surface state is observed within a superlattice gap. Varying the location of the terminating (surface) plane within a superlattice period causes this surface state to move across the gap for one half of the period and to disappear for the other half of the period. These observations are in good agreement with theoretical predictions.

PACS numbers: 73.20.At, 73.20.Dx, 79.60.Cn

The electronic properties of superlattices have been a subject of intense research in recent years. Much of the activity has focused on the bulk properties modified by the periodic modulation. Band folding and formation of superlattice gaps are well-known effects which have been demonstrated in many systems and utilized in various device applications. For surfaces of superlattices, much less has been done. An interesting issue is the possibility of new surface states existing within the superlattice gaps. This work is an angle-resolved photoemission study of a lattice-matched Ag-Au(111) superlattice. We have found a surface state, of the type described by Maue [1], Goodwin [2], and Shockley [3] (referred to as a Shockley state), within a superlattice gap. A unique feature of the superlattice geometry, as compared to ordinary single crystals, is that the location of the surface plane relative to the bulk can be experimentally varied within a superlattice period. This extra degree of freedom allows us to perform a critical test of the properties of this surface state. Namely, the system can be systematically modified from being "Shockley inverted" to being "noninverted" [3–5], and the surface state can be made to move across the gap for one half of the period and to disappear for the other half of the period. Our experimental results are in good agreement with theoretical predictions based on a simple two-band model and a phase-shift analysis.

The photoemission measurements were carried out at the Synchrotron Radiation Center of the University of Wisconsin-Madison. The Ag-Au superlattice samples were fabricated *in situ* using standard molecular-beam-epitaxy techniques. Briefly, Ag and Au were evaporated from separate tungsten crucibles heated with feedback controlled electron beams. A motorized mechanical shutter controlled by a computer allowed precise timing of the deposition. The rate of deposition was determined by a water-cooled quartz thickness monitor. The superlattices were grown on a Ag(111) substrate held at temperatures between 25 and 50 °C. High-energy electron diffraction, Auger spectroscopy, and core-level photoemission were employed for sample characterization.

A large number of samples with various superlattice periods and various Ag-Au slab-thickness ratios have been examined. Because of space limitations, we will concentrate on the results for a system with a 12-monolayer (ML) period and a Ag:Au slab-thickness ratio of 2:1. Figure 1 shows a set of normal-emission spectra, for various photon energies, taken from a Ag-terminated sample (i.e., a sample terminated by a full slab of 8 ML of Ag). The assignment of the spectral features in Fig. 1 is straightforward based on existing understandings of the angle-resolved photoemission technique [6,7]. The large peak just below the Fermi level is also observed on clean Ag(111) and corresponds to the well-known L-gap sur-

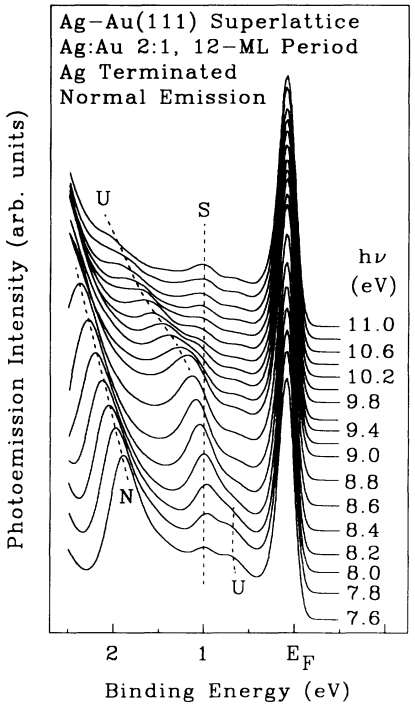

FIG. 1. Normal-emission spectra for a Ag-Au superlattice taken with various photon energies as indicated. The dashed curves serve as guides to the eye for the various peaks in the spectra. The binding-energy scale is referred to the Fermi level at E_F.

face state [8]. A similar state also exists on Au(111), with a somewhat different energy. This L gap, intrinsic to bulk Ag and Au, is unrelated to the superlattice configuration. The surface state seen in Fig. 1 is Ag(111)-like because the surface is Ag terminated. For a Au-terminated sample, this surface state shifts down by about 0.2 eV and becomes more Au(111)-like [9].

The peak labeled N (for normal) in Fig. 1 has a counterpart in both clean Ag(111) and Au(111); its movement toward lower binding energies for decreasing photon energies corresponds to the mapping of the sp valence band (the lower branch of the L gap) [7,10]. Following standard band-mapping technqiues [6,7,10], the dispersion is plotted in Fig. 2 using diamonds. Also shown in the figure are the corresponding Ag and Au sp valence bands (dashed curves) for comparison [6]; apart from an energy offset, these bands are very similar. The superlattice band is much closer to the Ag band than the Au band, because the material is overall Ag rich. The wave vector (abscissa) in Fig. 2 is measured in terms of $k_{\Gamma L}$, the wave vector connecting the Γ and L points in the bulk Ag (Au) Brillouin zone. The vertical dash-dotted lines indicate the locations of Bragg planes of the superlattice.

The weaker features S and U in Fig. 1 have no counterparts in either Au(111) or Ag(111); that is, these features are unique to the superlattice configuration [6–8,10]. Peak U is dispersive and is an umklapp peak arising from the same sp valence band. The corresponding band dispersion, after shifting by a reciprocal superlattice vector $k_{\Gamma L}/6$ to compensate for the umklapp transition, is shown in Fig. 2 by squares [7]. The squares and diamonds join smoothly, as they should, because they come from the same band. A superlattice gap is seen at $p \equiv (11/12)k_{\Gamma L}$, around which two U peaks appear simultaneously in the spectra and show the characteristic behavior of band mapping across a gap. In Fig. 2, the branch of the dispersion curves above the gap can be mapped only over a limited range in k space, and therefore its energy dispersion is not apparent (a significant energy dispersion can be observed for a shorter superlattice period) [7]. Peak S in Fig. 1 is dispersionless. Its energy position is slightly above the lower edge of the superlattice gap (indicated by a horizontal line in Fig. 2). The only possible assignment for it is a surface state within the superlattice gap [11].

The bulk bands remain unchanged as the surface termination of this superlattice is varied. Peak S remains dispersionless as a function of photon energy, but its energy position shifts as the surface termination is varied. Figure 3 shows the movement of S within the superlattice gap. Starting from the bottom spectrum which is for the Ag-terminated surface, each successive spectrum corresponds to the addition of one atomic layer in going through one entire superlattice period. In this sequence, one sees that the surface state is initially near the bottom of the superlattice gap. It then moves across the gap for half of the superlattice period, and disappears for the oth-

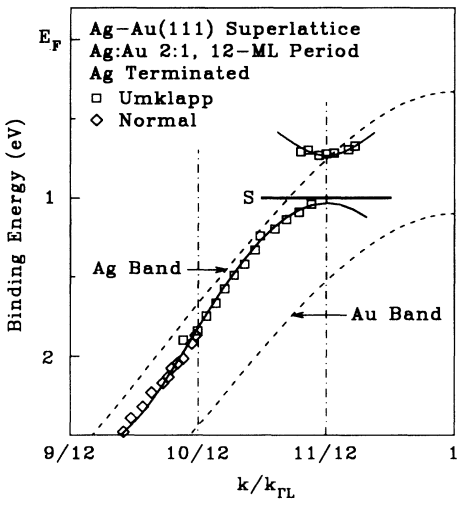

FIG. 2. Band dispersions derived from peaks U and N in Fig. 1. The squares and diamonds are data points, and the solid curves are guides to the eye. The dashed curves indicate the Ag and Au sp valence bands. The vertical dash-dotted lines indicate the locations of Bragg planes. The energy position of the surface state (S) is indicated by a horizontal line segment.

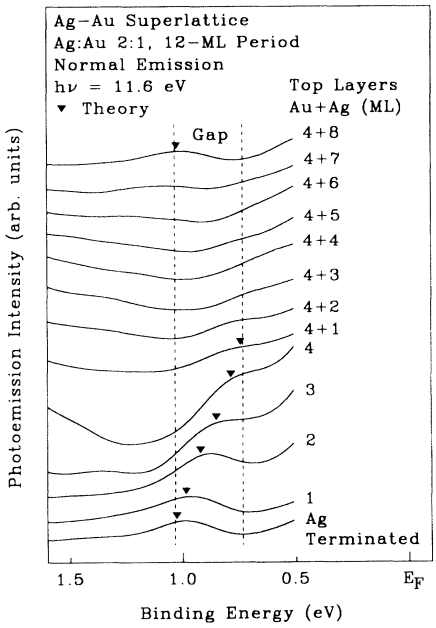

FIG. 3. Normal-emission spectra for various surface terminations of the superlattice taken with a photon energy of 11.6 eV. Starting from the bottom spectrum, which is for the Ag-terminated configuration, each successive spectrum corresponds to the addition of one atomic layer in going through one superlattice period. The top and bottom spectra correspond to the same sample configuration. The superlattice gap is indicated by two vertical dashed lines. The triangles indicate the energy positions of the surface state from our calculation.

er half of the superlattice period. The top spectrum represents a return to the original configuration after one full period of growth, and the spectrum is indeed reproduced. The behavior of this surface state is consistent with a model calculation (see below). The triangles in Fig. 3 indicate the calculated positions of this surface state, which are in fairly good agreement with the experiment (taking into account the background under each peak). The fifth spectrum in Fig. 3, counting up from the bottom, corresponds to a Au-terminated sample. This spectrum shows a rising background on both ends. On the low-binding-energy end, this is due to the tail of the intense L-gap surface state which has moved to lower binding energies. On the high-binding-energy end, this is due to the tail of the Au $5d$ emission which becomes more intense with Au termination.

We can only give a brief outline of our calculation here. The main ingredients, the two-band model and a phase-shift analysis, are well known [4]; these are modified and adapted here for an application to the superlattice configuration. The condition for the existence of a surface state is $r_B \exp(i\phi_B) r_C \exp(i\phi_C) = 1$, where r is the reflection coefficient, ϕ is the phase shift, and B and C denote the vacuum barrier and the crystal surface, respectively. This leads to $r_B = r_C = 1$; namely, the electron wave bouncing back and forth between the crystal surface and the vacuum barrier is not attenuated upon each reflection. This is satisfied for energies within the gap. Also, $\phi_B + \phi_C = 2n\pi$, where n is an integer. To calculate ϕ_C, we use the standard two-band formalism of the nearly-free-electron approximation. The input parameters are derived from a fit to the superlattice band structure near the gap (Fig. 2) using Eq. (3) of Ref. [12]. The fit yields a crystalline effective mass $m^*/m = 1.55$ and a gap of 0.30 eV. The effective mass is related to the curvature of the bands; it is included here for a first-order correction of multiband effects. These parameters are then used to calculate ϕ_C by matching the wave functions on the two sides of the surface plane [see Eq. (15) of Ref. [4]]. The vacuum barrier phase shift is determined by $\phi_B = (2/\hbar)\int [2m(E-U)]^{1/2} dz - \pi$, where E is the electron energy, U is the barrier potential, and the range of integration is from $z = z_0$ (surface plane) to the classical turning point. At large z, U approaches the image potential. Here, we take the image plane location derived from a density-functional jellium calculation [13]. At $z = z_0$, U equals the bottom of the crystal inner potential. In between (to so-called selvage region), the surface dipole layer gives rise to an approximately linear potential variation [13]. Thus, we construct U in the selvage region by using a linear potential tangent to the image potential. This construction takes into account the essential physics of the vacuum barrier, and leads to a ϕ_B in excellent agreement with the empirical rule described in Ref. [4]. The calculated $\phi_B + \phi_C$ is shown in Fig. 4 for the various terminations. Solutions for surface states are located at

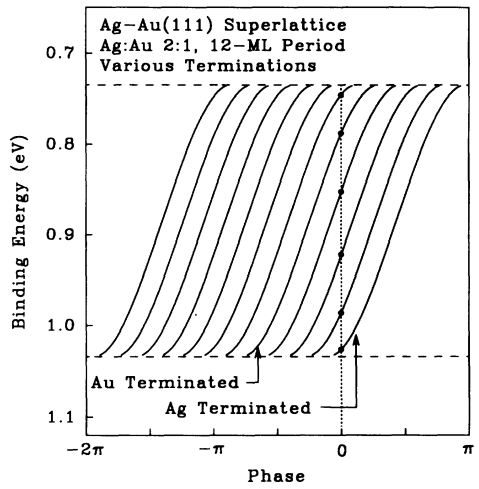

FIG. 4. Calculated phase shift $\phi_B + \phi_C$ vs the binding energy relative to the Fermi level. Starting from the rightmost curve, which is for the Ag-terminated configuration, each successive curve to the left corresponds to the addition of one atomic layer in going through one superlattice period. The two horizontal dashed lines indicate the gap.

points where the total phase is zero (indicated by the circles in Fig. 4), which are also indicated in Fig. 3 by the triangles.

The pattern of the curves in Fig. 4 can be easily understood. The gap, or the energy range of interest, is very small, so $\phi_B \approx$ const. Equation (15) of Ref. [4] leads to $\phi_C \approx 2pz_0 + 2\delta$, where δ is the phase factor of the gap state. The S shape of each curve in Fig. 4 reflects the variation of 2δ from $-\pi$ to 0 from the bottom to the top of the gap [4]. Neighboring curves are separated by just $2pd$ (d is the interlayer spacing), or $-\pi/6$, which arises from the phase variation of the crystal wave function at the surface-plane boundary as a function of z_0. Because of this $-\pi/6$ shift, it is clear from Fig. 4 that the surface state can only be observed for one half of the superlattice period, but not the other half. An equivalent way to view the problem is to note that a surface state exists only for a Shockley-inverted potential [3–5]; namely, the sinusoidal part of the crystal wave function must have a slope of the correct sign at the boundary for a match to the decaying solution on the vacuum side. If the potential (and the crystal wave function) is shifted in space by half a period relative to the surface, the sign of the slope will be inverted and matching becomes impossible [14]. Thus, it is a fairly general rule that for each terminating configuration supporting a surface state, adding half a period on top of the surface removes the surface state.

Note that the spectrum for the surface terminated with 7-ML Ag in Fig. 3 appears to show a broad and weak peak just outside the gap. This can be attributed to a surface resonance representing the analytic continuation of the surface state to beyond the gap. It follows the cal-

culation in a natural way. For energies outside the gap, $\phi_B+\phi_C=2n\pi$ is still possible, but r_C becomes less than 1, causing delocalization. A resonance state can exist if r_C is close to 1, namely, for energies near the gap. The detailed calculations will be presented in a complete paper in the future.

In summary, a Shockley-type surface state has been found in a Ag-Au superlattice gap. This system has a simple electronic structure allowing an analytic treatment. Our model calculation using parameters derived from the measured bulk band dispersions yields results in good agreement with the observation. This work illustrates some basic effects associated with superlattice modulation and electronic states on surfaces. A novel aspect is that the surface termination can be varied in a simple and systematic manner.

This material is based upon work supported by the U.S. National Science Foundation under Grant No. DMR-89-19056. Acknowledgment is also made to the Donors of the Petroleum Research Fund, administered by the American Chemical Society, and to the Department of Energy (Division of Materials Sciences, Office of Basic Energy Sciences), under Grant No. DEFG02-91ER45439, for partial personnel and/or equipment support. We acknowledge the use of central facilities of the Materials Research Laboratory of the University of Illinois, which is supported by the U.S. Department of Energy (Division of Material Sciences, Office of Basic Energy Sciences), under Grant No. DEFG02-91ER45439, and the U.S. National Science Foundation under Grant No. DMR-89-20538. The Synchrotron Radiation Center of the University of Wisconsin-Madison is supported by the U.S. National Science Foundation.

[1] A. W. Maue, Z. Phys. **94**, 717 (1935).

[2] E. T. Goodwin, Proc. Cambridge Philos. Soc. **35**, 205 (1939).

[3] W. Shockley, Phys. Rev. **56**, 317 (1939).

[4] N. V. Smith, Phys. Rev. B **32**, 3549 (1985), and references therein. There is a typographic error in Eq. (12); a factor of 2 should be added to the right-hand side. Also, z should be replaced by $z-z_0$ in Eq. (14).

[5] F. Forstmann, in *Photoemission and the Electronic Properties of Surfaces,* edited by B. Feuerbacher, B. Fitton, and R. F. Willis (Wiley, New York, 1978), pp. 193–226.

[6] *Photoemission of Solids,* Landolt-Börnstein: Numerical Data and Functional Relationships in Science and Technology, New Series, Group III, Vol. 23, edited by A. Goldmann and E. E. Koch (Springer-Verlag, Berlin, 1989).

[7] T. Miller, M. A. Mueller, and T.-C. Chiang, Phys. Rev. B **40**, 1301 (1989).

[8] See, for example, R. Courths, H. Wern, U. Hau, B. Cord, V. Bachelier, and S. Hüfner, J. Phys. F **14**, 1559 (1984).

[9] T. C. Hsieh and T.-C. Chiang, Surf. Sci. **166**, 554 (1986).

[10] See, for example, J. G. Nelson, S. Kim, W. J. Gignac, R. S. Williams, J. G. Tobin, S. W. Robey, and D. A. Shirley, Phys. Rev. B **32**, 3465 (1985).

[11] It has been pointed out to us that the dispersionless peak S bears some similarities to the quantum-well states observed in Ag overlayers on Au or Cu (see Ref. [12]). This leads to the question of whether or not our data can be explained by a simple quantum-well model. The answer is no because such a model cannot explain, in a consistent manner, both features U and S in the spectra. In particular, the observed energy dispersion of peak U is completely incompatible with a simple quantum-well model.

[12] M. A. Mueller, T. Miller, and T.-C. Chiang, Phys. Rev. B **41**, 5214 (1990).

[13] N. D. Lang and W. Kohn, Phys. Rev. B **7**, 3541 (1973).

[14] See Fig. 8.4 in Ref. [5]. Also, see Fig. 4.10 in Andrew Zangwill, *Physics at Surfaces* (Cambridge Univ. Press, New York, 1988), p. 65.